Stokes Reflectometer for Soil Moisture, Subterranean Voids, and Subsurface Ice

Mary R. Keller, Andrew C. Strikwerda, Joshua T. Cahill, Lauren M. Jozwiak, Brian C. Montgomery, Nelofar Mosavi, Michael E. Nord, Wes Patterson, Hermann Sequeira, Angela M. Stickle, and Dalibor J. Todorovski

Abstract – The Stokes reflectometer concept presented here takes a novel approach to microwave remote sensing of soils. It relies on a constellation of low-power, low-mass, continuous wave, ultrahigh-frequency transmitters and receivers. The systems are arranged in a forward scattering configuration over a range of angles of incidence and scattering set to cross the Brewster angle to retrieve soil properties. Proof of concept is provided by a series of COMSOL Multiphysics finite element runs to model Stokes parameters (SP) of forward-scattered RF signals through layers of varying compositions, dielectric constants, and surface roughness, assuming no sources of contamination during transmission. Significant variations for all four SP were demonstrated. At frequencies around 430 MHz, contamination during transmission is due to Faraday rotation (FR) in the ionosphere. A hybrid-polarimetric configuration minimized ionospheric contamination and provided for simplified expressions to retrieve FR angles and scattering coefficients from the received polarimetric power. With these, SP can be correctly calculated to soil moisture retrievals.

1. Introduction

As the atmosphere changes in response to global temperature rise, extreme rain events are becoming more common. Further, they are occurring at times and in locations unpredicted by climatology. Once the rains stop, soils remain saturated and can slump in large-scale mudslides that bury homes and harm their occupants.

Satellite-based remote sensing, with its frequent repeats, has the potential for timely soil-moisture measurement updates on areas that pose threats to populated regions and otherwise inaccessible terrain. Existing satellite systems addressing soil moisture have taken multiple approaches. To retrieve soil moisture data, L-band passive microwave systems were launched: European Space Agency–Soil Moisture and Ocean Salinity–Microwave Imaging Radiometer with Aperture Synthesis (ESA-SMOS-MIRAS) [1] and National Aeronautics and Space Administration–Soil Moisture Active/Passive (NASA-SMAP) [2]. The L-band Cyclone Global Navigation Satellite System (CyGNSS) receivers, designed to capture GNSS signals of opportunity, were originally intended to retrieve hurricane wind data but will be applied to soil moisture as well [3]. A soon-to-be-launched CubeSat mission to measure soil moisture at P-band (240–380 MHz), SigNals of OppOrtunity: P-band Investigation (SNOOPI), will also use signals of opportunity [4]. Efforts have been taken to use the C-band synthetic aperture radar (SAR) systems of the RADARSAT Constellation Mission (RCM) and the Sentinel-1 SAR constellations for soil moisture retrievals. But at L- and C-bands, surface roughness from vegetation can have an order-of-magnitude-stronger effect on the Fresnel reflection coefficients than soil moisture [5, 6].

The Stokes reflectometer (SR) system presented in this short article offers a different approach from all of these. It is a constellation of inexpensive hybrid-polarimetric RF systems transmitting narrowband P-band frequencies over a range of incident angles to retrieve soil properties via the Stokes parameters (SP). The transmitter frequencies cluster around 430 MHz. Here, surface roughness and vegetation signatures are reduced relative to soil moisture response, so soil moisture values are retrieved more easily. But at ultrahigh frequencies, contamination from the ionosphere becomes significant and must be addressed.

The remainder of this article is divided into several sections. Section 2 provides further details on the SR concept of operations. Section 3 calculates expected SP signatures for varied soil moisture conditions given an atmosphere free of contamination effects. Section 4 models the strength of Faraday rotation (FR) at 430 MHz for our system configuration; it also derives polarimetric equations to extract the surface scattering coefficients and FR angles from measured hybrid polarimetric powers.

2. SR System Approach

The basic approach used by the SR, sub-500 MHz transmission of forward-scattered signals around the Brewster angle that are inverted to derive soil properties, was demonstrated using the telemetry carrier from Explorer 35 in Lunar orbit [7]. The 136.11 MHz carrier was single circular polarization at time of

Manuscript received 29 August 2020.

Mary R. Keller, Andrew C. Strikwerda, Joshua T. Cahill, Lauren M. Jozwiak, Brian C. Montgomery, Nelofar Mosavi, Michael E. Nord, Wes Patterson, Hermann Sequeira, Angela M. Stickle, and Dalibor J. Todorovski are with the Johns Hopkins University/Applied Physics Laboratory, Laurel, Maryland 20723, USA; e-mail: Mary.Keller@jhuapl.edu, Andrew.Strikwerda@jhuapl.edu, Josh.Cahill@jhuapl.edu, Lauren.Jozwiak@jhuapl.edu, Brian.Montgomery@jhuapl.edu, Nelofar.Mosavi@jhuapl.edu, Michael.Nord@jhuapl.edu, Wes.Patterson@jhuapl.edu, Hermann.Sequeira@jhuapl.edu, Angela.Stickle@jhuapl.edu, Dalibor.Todorovski@jhuapl.edu.

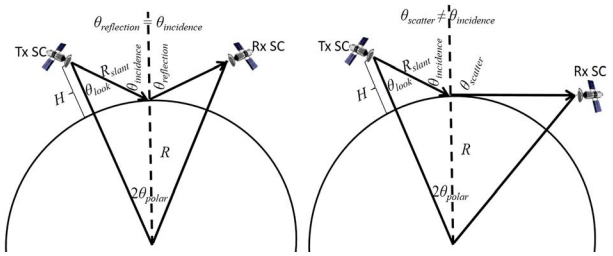

Figure 1. (Left) Bistatic specular reception is used for soil moisture estimation; (right) bistatic specular and nonspecular reception provide depth profiles.

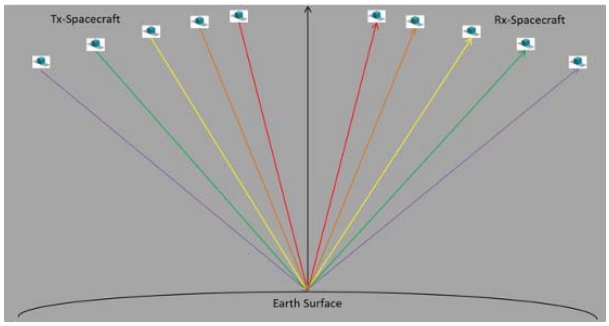

Figure 2. Simple satellite formation at nominal 400 km altitude. All spacecraft travel at Mach 23 in single file along a common orbital trajectory. Further details are in Table 1.

transmit to avoid the effects of FR in Earth's ionosphere. The forward-scattered signal, Doppler broadened due to the rough surface scatter and the platform motion, was integrated for total received power. The reflectivity was derived using the radar equation and shown to minimize at the Brewster angle. The retrieved effective dielectric constant was 3.0 $\pm$ 0.2, in the range expected for the maria and highlands.

The smallest element of the SR is a bistatic pair of platforms in which the reception platform receives a signal scattered off a spot on Earth's surface that is illuminated by a transmitting platform. Such a bistatic pair is referred to as an arrangement of platforms. As Figure 1 shows, we have a specular arrangement for which the usual Fresnel laws of reflection and refraction apply and a nonspecular arrangement for which scattering occurs due to surface roughness and from electromagnetic inhomogeneity beneath the surface. Such scattering also affects the specular characteristics of the received signal. By analyzing the signature embodied in the components of the Stokes vector, we derive characteristics of surface and subsurface compositions.

When multiple pairs are flown, the arrangements are referred to as a formation, as illustrated in Figure 2, where the incident angles (Table 1) are identified by frequency (depicted with color) of the signal. Every transmitter is set to a different frequency, so the scattering pairing and incident angle can be known automatically, thus eliminating the need for time synchronization for operation. Unlike existing SARs or scatterometers, each transmitter emits a narrowband continuous wave (CW) signal that affords lower transmitter power. Unlike SAR antennas, the patterns of the crossed transmit and receive fan beam antennas provide smaller two-dimensional spatial overlap on the ground, which gains better resolution than either fan beam can provide alone. At the same time, each fan beam provides wide angular coverage and enables signal acquisition over a large span of incident angles, that is, from the other pairs in the formation.

Table 2 compares the SR with existing soil moisture systems. Note that SR has the best horizontal resolution of all the systems and provides the most flexibility for operating conditions. Unlike the SNOOPI and CyGNSS systems, the SR design can shift frequencies to avoid interference from other sensors since the precise frequency of each pair is chosen only to indicate incident angle. Thus, although frequencies around those used by the US Space Objects Tracking Radar [8] are reported, the frequencies of the operational SR pairs will be adjusted to avoid data loss. The resulting signal characteristics will not be significantly different from those reported here. The SNOOPI and CyGNSS instruments are locked into their frequencies and bandwidths because they are receiving transmissions from preexisting systems.

Resource demands of the payload on each platform are a function of resolution required of the payload. For weather-cell scale resolution of the order of tens of kilometers, the payload weighs 14 kg, consumes 21 W of power, and generates data at a rate of 8.6 kbps. If the application demands resolution of the order of a few meters, the payload weighs 25 kg, consumes 85 W of power, and generates data at a rate of 8.6 Mbps.

3. Soils Modeling for Stokes Parameters

Careful measurements of soils and their dielectric properties have been and are continuing to be conducted by researchers over the past and present decades [9, 10]. However, only recently have finite element methods evolved to rapidly calculate electromagnetic properties from mixed layers of soils, voids, and snow/ice with different dielectrics. One such system is COMSOL Multiphysics version 5.4 (COMSOL Inc.), a cross-platform finite element analysis, solver, and multiphysics simulation software [11].

A model volume for the subsurface was created to calculate SP for the SR. The model geometry positioned the origin for the frame of reference horizontally in the center of the top surface of the uppermost layer and vertically at the mean level of the top surface of the uppermost layer. The width of the simulation is set to contain 99% of the beam power. Absorbing layers surround the simulation domain to eliminate refraction out of or multiple reflections in the model volume.

The SR antenna beam is assumed Gaussian. The center of the intersection of the beam with the top

Table 1. Slant range to the illuminated position and the arc separation between adjacent spacecraft. Each specular pair is identified by the same subscripted index

	Satellite transmitter and receiver									
	Tx_5	Tx_4	Tx_3	Tx_2	Tx_1	Rx_1	Rx_2	Rx_3	Rx_4	Rx_5
θ^o_{look}	60.13	52.24	43.62	34.64	30.05	30.05	34.64	43.62	52.24	60.13
θ^o_{inc}	67	57	47	37	32	32	37	47	57	67
R_{slant} (km)	899.32	691.54	569.32	493.66	467.10	467.10	493.66	569.32	691.54	899.32
Arc separation (km)	249.15	164.02	119.43	49.60	497.34	497.34	49.60	119.43	164.02	249.15

surface of the uppermost layer is at the origin of the frame of reference. The peak amplitude of the beam is 1 V/m. The beamwidth is set to 10 wavelengths. The SR frequency is kept at 430 MHz. Model runs for transverse electric and transverse magnetic polarization were at the incident angles listed in Table 1, then SP were calculated from the results.

The soil surface was assumed to be untilled. The distribution of surface scales was modeled with Fourier components whose Fourier coefficients A_n and phases are random but are controlled by the fractal dimension f_D used. The magnitude of A_n decreases with increasing n. The Fourier sum is truncated to eliminate spatial features smaller than a wavelength. The surfaces of the layers above and below the soil surface are correlated, with the exception of the snow layer, if it is present. For snow, only low-n terms are used to capture the smoothness typical of the air/snow interface.

Layers with different dielectrics and soil moistures were established in the volume prior to calculations. Table 3 lists the dielectric properties of the different layers used in the simulations. Two generalized configurations were examined for different values of f_D. Configuration 1 stacked 30 cm of saturated soil above an infinite (in model geometry) layer of dry soil. Configuration 2 stacked 4 m of snow above 1 m of ice above 20 cm of saturated soil above an infinite layer (in model geometry) of dry soil.

Fractal analysis has been shown to more completely characterize multiscaled soil surfaces [12] than does assuming a single-scale process with one root mean square height and correlation length. Three f_D values were applied to each of the two configurations: a smooth surface ($f_D = 1$), a surface with $f_D = 1.5$, and a surface with $f_D = 1.7$. A value of 1.5 for f_D is equivalent to a soil profile with an exponential correlation function [13]. These fractal dimensions are typical of the three-dimensional roughness of a sandy clay loam worked with chisels to replicate wind and rain disturbance [14].

To acquire valid statistics, 50 runs for each combination of generalized configuration and controlling f_D were performed. For each of these 300 runs, a different random seed was used. The reflected SP versus angle were recorded. Means and standard deviations were calculated for each combination of SP, incident angle, generalized configuration, and f_D.

Figures 3 and 4 show the means of S0 and S3 for configuration 1. Any soil roughness roughly doubles the Stokes magnitude at all incident angles over the smooth surface case $f_D = 1$. The $f_D = 1.5$ case is clearly distinguishable from $f_D = 1.7$. Figure 5 shows the means of S0 for configuration 2. While the difference of the relative magnitudes of the smooth surface versus the roughest surface was similar to Figure 3, there is now little differentiation between the $f_D = 1.5$ and the $f_D = 1.7$ roughness cases. The additional moisture in the surface layers was sufficient to mask roughness changes, as is expected for these ultrahigh frequencies.

4. Ionospheric Effects

Estimation of soil moisture depends on 1) changes in polarization state of the wave as it bounces off Earth's surface and 2) the absence of contamination of its polarization state as it propagates toward and away from Earth's surface. The ionosphere is a dominant contributor to such contamination. The SR operates at frequencies between 424 MHz and 435 MHz, where attenuation, refraction, and scintillation effects are negligible [15]. The dominant effect is FR and the differential phase retardation that it causes. FR is the change in orientation of the plane of polarization of a linearly polarized electromagnetic wave. Such a wave may be considered as composed of right circularly polarized and left circularly polarized components. When these components traverse a plasma, a relative phase retardation develops between them that causes their recombination to a linear polarization whose plane is rotated relative to that of the entering beam. By

Table 2. Comparison of SR with existing soil moisture measurement systems

Sensor	SMOS	SMAP	CyGNSS	SNOOPI	SR
Horizontal resolution (km)	50	9	0.6 along-track	0.81	0.008 (using spatial sharpening)
Penetration depth (cm)	5	5	5	10–20	10–20
System type	Radiometer	Radiometer	Signals of opportunity receiver	Signals of opportunity receiver	Selectable transmit/receive narrowband RF
Polarization	H, V	Polarimetric H, V	L, R	Dual linear	Hybrid polarimetric

Table 3. Multilayer soil moisture modeling parameters

Layers from top to bottom	Thickness (m)		Dielectric permittivity	Conductivity (μs/m)	Skin depth
	Configuration 1	Configuration 2			
Snow	Not used	4.0	2.4	0	Infinite
Ice (freshwater)	Not used	1.0	3.3	1	9.644 km
Saturated soil	0.3	0.2	31.0	10	2.96 m
Dry soil	∞	∞	5.5	100	124.5 m

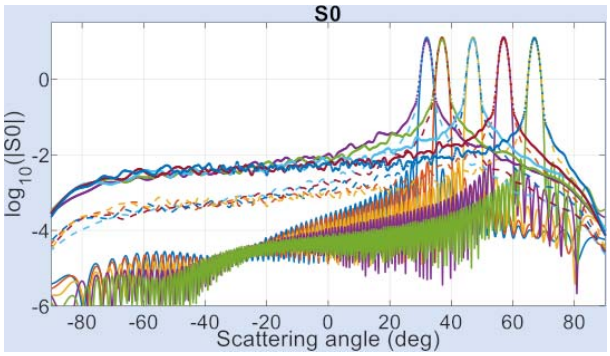

Figure 3. Mean first SP for saturated soil layer on dry soil (configuration 1 in Table 3). Upper solid lines are $f_D = 1.7$, dashed lines are $f_D = 1.5$, lower solid lines are smooth soil, and $f_D = 1$. Table 1 lists θ_{inc}, distinguishable by specular peak locations.

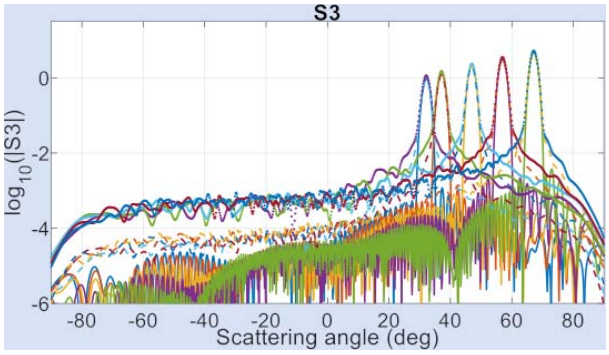

Figure 4. Mean fourth SP for saturated soil layer on dry soil. Annotation as in Figure 3.

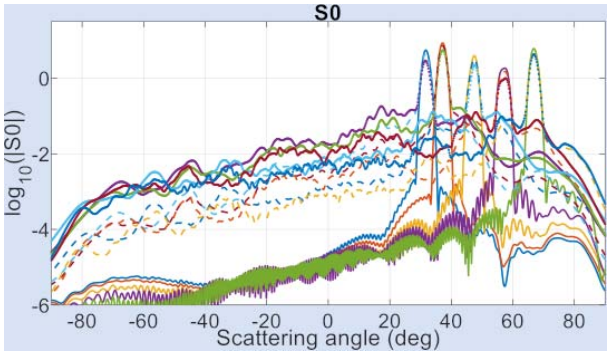

Figure 5. Mean first SP for snow on ice on saturated soil on dry soil (configuration 2 in Table 3). Annotation as in Figure 3.

choosing to transmit circularly and receive linearly [16], the FR effects are restricted to the path between the surface and the receiver. Table 4 shows the FR angles expected in this case. Clearly, FR is nonnegligible around 430 MHz.

The governing equation for hybrid-polarimetric forward scattering from moist soils can be written following the method of [15]:

$$\begin{bmatrix} E_H \\ E_V \end{bmatrix} = \begin{bmatrix} 1 & 0 \\ 0 & 1 \end{bmatrix} \frac{1}{\sqrt{2}} \begin{bmatrix} \cos\Omega & \sin\Omega \\ -\sin\Omega & \cos\Omega \end{bmatrix} \begin{bmatrix} S_{hh} & S_{hv} \\ -S_{vh} & S_{vv} \end{bmatrix} \begin{bmatrix} 1 & 1 \\ -j & j \end{bmatrix} \begin{bmatrix} E_R \\ E_L \end{bmatrix} \tag{1}$$

where E with single subscripts and S with double subscripts are the polarimetric components of the (complex) electric field and of the scattering matrix, respectively, and the FR angle is Ω. Note that only one rotation matrix is used. Rationalization and short-term averaging to eliminate uncorrelated phase terms produce a set of four equations for the measured powers:

$$P_{hh} = \cos^2\Omega\sigma^0_{hh} + \sin^2\Omega\sigma^0_{vh} \tag{2}$$

$$P_{vh} = \cos^2\Omega\sigma^0_{vh} + \sin^2\Omega\sigma^0_{hh} \tag{3}$$

$$P_{hv} = \cos^2\Omega\sigma^0_{hv} + \sin^2\Omega\sigma^0_{vv} \tag{4}$$

$$P_{vv} = \cos^2\Omega\sigma^0_{vv} + \sin^2\Omega\sigma^0_{hv} \tag{5}$$

Basic trigonometric relations can now be used to separate the scattering coefficients σ^0_{pq}, where pq represent linear polarizations from the FR terms. With the scattering coefficients measured, the components of the scattering matrix are calculated. SP can then be written from the received electric field using equations similar to (1) but minus the now unnecessary FR matrix.

5. Conclusions

A low-power, low-mass, CW, ultrahigh-frequency system of transmitters and receivers to retrieve soil properties is presented. They operate in a forward scattering configuration over a range of angles of incidence and scattering that cross the Brewster angle. Proof of concept for the SR is provided by a series of COMSOL Multiphysics finite element runs. The calculations model the SP of forward-scattered RF

Table 4. FR number (1.0 = 360°) from ionospheric propagation in the hybrid-polarimetric case

	Frequency (MHz)									
	Forward-looking					Backward-looking				
Incidence (°)	423.94	423.97	424.00	424.03	424.06	434.94	434.98	435.01	435.04	435.07
37	0.722	0.722	0.722	0.722	0.722	0.686	0.686	0.686	0.686	0.686
47	0.735	0.735	0.735	0.735	0.734	0.698	0.698	0.698	0.698	0.698
57	0.821	0.821	0.820	0.820	0.820	0.780	0.780	0.779	0.779	0.779
67	0.940	0.940	0.940	0.940	0.940	0.893	0.893	0.893	0.893	0.893
77	1.066	1.066	1.066	1.066	1.066	1.013	1.013	1.013	1.013	1.012

signals through layers of varying compositions, dielectric constants, and surface roughness, assuming no sources of contamination during transmission. At frequencies around 430 MHz, contamination during transmission is due to FR in the ionosphere. A hybrid-polarimetric configuration minimized ionospheric contamination. It also provided for simplified expressions to retrieve FR angles and scattering coefficients from the received polarimetric power. With these coefficients, SP free of FR effects can be generated for soil moisture retrievals.

6. References

1. Y. H. Kerr, P. Waldteufel, J.-P. Wigneron, S. Delwart, F. Cabot, et al., "The SMOS Mission: New Tool for Monitoring Key Elements of the Global Water Cycle," *Proceedings of the IEEE*, **98**, 5, May 2010, pp. 666-687, doi: 10.1109/JPROC.2010.2043032.
2. L. Fang, X. Zhan, J. Yin, J. Liu, M. Schull, et al., "An Intercomparison Study of Algorithms for Downscaling SMAP Radiometer Soil Moisture Retrievals," *Journal of Hydrometeorology*, **21**, 8, August 2020, pp. 1761-1775, https://doi.org/10.1175/JHM-D-19-0034.1.
3. O. Eroglu, M. Kurum, D. Boyd, and A. C. Gurbuz, "High Spatio-Temporal Resolution CYGNSS Soil Moisture Estimates Using Artificial Neural Networks," *Remote Sensing*, **11**, 19, 2272, September 2019, https://doi.org/10.3390/rs11192272.
4. J. L. Garrison, J. Piepmeier, R. Shah, M. A. Vega, D. A. Spencer, et al., "SNOOPI: A Technology Validation Mission for P-Band Reflectometry Using Signals of Opportunity," IGARSS 2019, 2019 IEEE International Geoscience and Remote Sensing Symposium, Yokohama, Japan, July 28–August 2, 2019, pp. 5082-5085, doi: 10.1109/IGARSS.2019.8900351.
5. C. Ma, X. Li, and M. F. McCabe, "Retrieval of High-Resolution Soil Moisture Through Combination of Sentinel-1 and Sentinel-2 Data," *Remote Sensing*, **12**, 14, 2303, July 2020, doi: 10.3390/rs12142303.
6. A. Merzouki, H. McNairn, J. Powers, and M. Friesen, "Synthetic Aperture Radar (SAR) Compact Polarimetry for Soil Moisture Retrieval," *Remote Sensing*, **11**, 19, 2227, September 2019, doi: 10.3390/rs11192227.
7. G. L. Tyler, "Oblique-Scattering Radar Reflectivity of the Lunar Surface: Preliminary Results From Explorer 35," *Journal of Geophysical Research*, **73**, 24, December 1968, pp. 7609-7620, doi: 10.1029/JB073i024p07609.
8. S. Yueh, R. Shah, X. Xu, K. Elder, and B. Starr, "Experimental Demonstration of Soil Moisture Remote Sensing Using P-Band Satellite Signals of Opportunity," *IEEE Geoscience and Remote Sensing Letters*, **17**, 2, February 2020, pp. 207-211, doi: 10.1109/LGRS.2019.2918764.
9. P. Hoekstra and A. Delaney, "Dielectric Properties of Soils at UHF and Microwave Frequencies," *Journal of Geophysical Research*, **79**, 11, April 1974, pp. 1699-1708, doi: 10.1029/JB079i011p01699.
10. N. R. Peplinski, F. T. Ulaby, and M. C. Dobson, "Dielectric Properties of Soils in the 0.3-1.3-GHz Range," *IEEE Transactions on Geoscience and Remote Sensing*, **33**, 3, May 1995, pp. 803-807, doi: 10.1109/36.387598.
11. COMSOL Inc., *COMSOL Multiphysics Reference Manual*, Burlington, MA, COMSOL, 2018, http://doc.comsol.com/5.4/doc/com.comsol.help.comsol/COMSOL_Reference Manual.pdf (Accessed 19 January 2021).
12. M. W. J. Davidson, T. Le Toan, F. Mattia, G. Satalino, T. Manninen, et al., "On the Characterization of Agricultural Soil Roughness for Radar Remote Sensing Studies," *IEEE Transactions on Geoscience and Remote Sensing*, **38**, 2, March 2020, pp. 630-640, doi: 10.1109/36.841993.
13. M. Zribi, V. Ciarletti, and O. Taconet, "Validation of a Rough Surface Model Based on Fractional Brownian Geometry With SIRC and ERASME Radar Data Over Orgeval Site," *Remote Sensing of the Environment*, **73**, 1, July, 2000, pp. 65-72, doi: 10.1016/S0034-4257(00)00082-1.
14. R. G. Moreno, M. C. D. Álvarez, A. S. Requejo, and A. M. Tarquis, "Multifractal Analysis of Soil Surface Roughness," *Vadose Zone Journal*, **7**, 2, May 2008, pp. 512-520, doi: 10.2136/vzj2007.0016.
15. P. A. Wright, S. Quegan, N. S. Wheadon, and C. D. Hall, "Faraday Rotation Effects on L-Band Spaceborne SAR Data," *IEEE Transactions on Geoscience and Remote Sensing*, **41**, 12, December 2003, pp. 2735-2744, doi: 10.1109/TGRS.2003.815399.
16. R. K. Raney, "Hybrid-Polarity SAR Architecture," *IEEE Transactions on Geoscience and Remote Sensing*, **45**, 11, November 2007, pp. 3397-3404, doi: 10.1109/TGRS.2007.895883.